Heliyon 6 (2020) e03912

Contents lists available at ScienceDirect

Heliyon

journal homepage: www.cell.com/heliyon

Research article

Natural rubber modification as a pre-vulcanized latex impregnated with TiO_2 for photo-catalytic degradation of gaseous benzene

Peerapol Kaoien [a], Wipawee Dechapanya [a,*], Attaso Khamwichit [a], Kowit Suwannahong [b]

[a] School of Engineering and Technology, Walailak University, 222, Thai Buri, Tha Sala District, Nakhon Sri Thammarat Provicne, 80160 Thailand
[b] Faculty of Public Health, Burapha University, 169, Saensuk, Mueang Chon Buri District, Chon Buri Province, 20131 Thailand

ARTICLE INFO

Keywords:
Chemical engineering
Materials application
Environmental engineering
Environmental management
Environmental pollution
Benzene removal
Photocatalytic oxidation process
Air pollution treatment
Pre-vulcanized latex (PVL-TiO_2) film

ABSTRACT

Photocatalytic oxidation purposes an economical and environmental friendly process to remove benzene from indoor air pollution. However, the process efficiency is primarily dependent on catalytic-film. The main purpose of this study is to synthesize pre-vulcanized latex impregnated with TiO_2 (PVL-TiO_2 thin film) from natural rubber to be used in photo-catalytic oxidation for benzene removal in a reactor. PVL-TiO_2 thin films were synthesized for 3 different dosages of TiO_2, which were 5%, 15%, and 25% The outcome of this study offers the new application of modified natural rubber in terms of environmental and health care protection. Morphology of the synthesized films was analyzed by SEM. The results showed that TiO_2 particles could be well dispersed all over the surface of the film, in which the best distribution could be found for the PVL-TiO_2 15% thin film. Tensile stress of the films was analyzed using ASTM D412. Results showed that the stress of the films got higher with the increasing amount of TiO_2 content. This indicates that TiO_2 strengthened the PVL-TiO_2 film because the uniformly distribution of TiO_2 on the inner surface increased the strength of the film. The decomposition of PVL and PVL-TiO_2 thin films was analyzed using thermo gravimetric analysis. The maximum weight loss rates in the range of 1.536–1.145 wt %/°C attained at between 380 - 382 °C TiO_2 particles enhanced thermal stability of PVL-TiO_2 thin films due to the high decomposition temperature of its properties and also acted as barrier for the heat transfer of the films. Specific surface area (SSA) of the films was analyzed using Brunauer-Emmett-Teller. Specific surface area increased as the increasing content of TiO_2, which corresponded to the morphology analysis by SEM. The analysis of chemical functional group of thin films was performed using ATR-FTIR. The results of Crystal identification using XRD clearly showed good attachment of rutile TiO_2 on the films. Finally, results of absorbance spectrums and band gap energy showed that PVL not only peg TiO_2 particles but also reducing band gap energy which induced by S and ZnO. Therefore, PVL-TiO_2 thin films could be used under visible light condition. The films were then used in the study of benzene removal in annular reactor. The highest removal efficiency (83%)for the PVL-TiO_2 15% thin film was obtained. Comparing to the maximum removal efficiency for PVL film (28%), roughly 60% increase in efficiency was achieved. The PCO kinetics were well fit by a first order Langmuir-Hinshelwood model. The calculation of oxidation rate and percentage of residual intermediates indicated that accumulation of residual intermediates can occur on the active site and the gas phase, resulting in increasing of residual intermediates. The successful synthesis of PVL-TiO_2 thin film provides new opportunity to use natural rubber in terms of environmental and health care protection.

1. Introduction

Benzene (C_6H_6) is one of the most commonly emitted VOCs from vehicles, gas station, and from industrial facilities where using benzene as a solvent, [1, 2]. Benzene has shown the causing of severe health problems and environmental effects, due to its carcinogenic nature and its tendency to form secondary pollutants [3]. Although there are a number of alternative promising VOCs removal technologies such as adsorption [4], membrane separation [5], liquid absorption, plasma catalysis [6], biological degradation [1] and photo-catalytic oxidation [7]. However, each of them might be limited to be used with all types of VOC treatment. Photo-catalytic oxidation (PCO) is one of the most appropriate methods because it can potentially convert VOCs to water and carbon dioxide as end products [8]. Various advantages are that

* Corresponding author.
E-mail addresses: khamwipawee@gmail.com, kwipawee@wu.ac.th (W. Dechapanya).

https://doi.org/10.1016/j.heliyon.2020.e03912
Received 5 February 2020; Received in revised form 8 April 2020; Accepted 29 April 2020

could be operated at low pressures and temperatures, use inexpensive semi-conducting catalysts, and be applicable to the oxidation of a wide range of pollutants. Moreover, PCO has received considerable attention as a green alternative technology [9].

For PCO, one of the most important factors affecting its efficiency is a catalyst. Titanium dioxide (TiO_2) stands out as a particularly attractive photo-catalyst because it is abundant, inexpensive, and has high photo-catalytic activity [10]. In addition, it is non-toxic at most relevant exposure conditions [11]. Bui et al, 2011 revealed that an anatase form TiO_2 is higher active for the oxidation of benzene than a rutile form [12]. However, the stabilization of TiO_2 onto substrate is quite a challenge, the suspended particle tends to aggregate especially at high concentration [13]. To overcome these difficulties, development of pre-vulcanized latex impregnated with TiO_2 (PVL-TiO_2) thin film to be used as photo-catalytic supporter proposes an interesting and promoting technique of immobilizing catalyst on rubber thin film.

In terms of environmental use, previous studies reported the preparation of rubber sheet impregnated with titanium dioxide particles by direct mixing of TiO_2 powder into rubber latex (60% HA Concentrated Latex) to make rubber sheets for methylene blue solution degradation [11]. The result indicated that 99.89% degradation efficiency can be obtained and the impregnated rubber sheet can be reused more than four times [14]. Sriwong et al., (2012b) studied 3 techniques of preparation of the rubber sheet, impregnated with titanium dioxide, strewn with titanium dioxide and embedded impregnated with titanium dioxide. The result showed that photodegradation efficiency more than 90% was still achieved after 10 times of using [15]. The TiO_2 impregnated thin rubber sheets prepared by several techniques showed less efficiency than that of loose TiO_2 powder but it has one clear advantage over loose powder because it can be reused many times [16].

This study aims to synthesize PVL-TiO_2 thin films to be used for benzene removal from air via photocatalyatic oxidation process. Structures and physical properties of PVL-TiO_2 thin films were examined by analyzing the morphology, tensile stress, the decomposition rate of polymer, the functional groups of chemical structures, crystalline structures, UV-Visible absorbance spectra, and energy band gap. Finally, the efficiencies of benzene degradation via the photocatalytic oxidation process were analyzed using PVL-TiO_2 thin films.

2. Materials and methods

2.1. Synthesis of PVL-TiO_2 thin film

PVL-TiO_2 thin films were synthesized from natural rubber (NR) in the form of concentrated latex 60% by weight since it has high latex as well as low protein, carbohydrate and nitrogen [17]. To prepare the films, the concentrated latex 60% (w/w) was mixed with vulcanizing chemical reagents as shown in Table 1. PVL-TiO_2 solution was prepared by mixing concentrated latex 60% (w/w) with K-Oleate, TiO_2, Sulfur, Zinc Diethyl-dithio-carbamate (ZDEC) and Poly (dicyclopentadiene-co-p-cresol), respectively. The stirring time of 5 min was required for mixing individual chemicals into the solution. ZnO was added lastly and stirred for 2 h at room temperature, then stored at room temperature for 24 h of maturation. Aluminum foil sheets (size 26 × 62 cm^2) were prepared to be used as supporters of PVL-TiO_2 thin films. 30 grams of the PVL-TiO_2 solution was poured in a spray gun, the solution was sprayed on the prepared foils and dried in an open air for 24 h at room temperature (25 ± 3 °C) before drying in an oven at 60 °C for 3 h. Finally, the films were cooled down at room temperature (25 ± 3 °C). The preparation process of PVL-TiO_2 thin films is shown in Figure 1.

2.2. Characterization

Morphology of PVL-TiO_2 thin films were examined by a Scanning Electron Microscope (SEM, Model Merlin compact, Zeiss). The sample was mounted on aluminum stubs, sputter-coated with gold and examined in a Merlin compact scanning electron microscope. Samples were analyzed at 3,000X. Tensile stress of PVL-TiO_2 thin film was tested using the Universal Testing Machine-Tensile Tester (LLOYD Instruments), the analysis procedure followed ASTM D412 standard. Eight dumbbell samples were used in the test for PVL, 5%, 15%, and 25% PVL-TiO_2 thin films. Decomposition rate of PVL and PVL-TiO_2 thin film was estimated by a thermogravimetric analyzer (Perkin Elmer model TGA8000). Samples were heated from 35 °C to 800 °C at 10 °C/min in nitrogen. Specific surface area was reported as BET surface areas which were obtained by applying the theory of Brunauer, Emmett, and Teller to nitrogen adsorption isotherms measured at 77 K. Functional group of chemical structures of PVL and PVL-TiO_2 thin films were analyzed by a ATR-FTIR Spectrometer (Model Tensor 27, Bruker) using ATR-FTIR technique. The crystalline structures of TiO_2, PVL, and PVL-TiO_2 thin films were determined by the X-Ray Diffraction (XRD) analysis (X-Ray Diffractometer; Philips model X'Pert MPD). The current was adjusted to 40 mA. The voltage was increased to 40 kV. The reflection angle 2θ was in the range of samples 5^o to 90^o, time/step 1 s. The ultraviolet-visible spectra of the PVL-TiO_2 thin films was analyzed by the UV- Visible spectrophotometer (Jasco V-770 UV-Vis Spectrophotometer). The scan ranged from 200 to 800 nm. All spectrum was monitored in the absorbance mode and acquired under ambient conditions. The band gap energy of TiO_2 on a film was calculated from absorbance results [18].

2.3. Photo-catalytic oxidation reactor

Photocatalytic reactor design considers three principle factors including maximum flow rate, total system pressure drop, and power of gas pump [19]. Schematic of photocatalytic oxidation reactor system is shown in Figure 2. The reactor used in this study is an annular closed-system made of a stainless steel and consists of an ultraviolet lamp type C at 254 nm wavelength. The light intensity used in the experiments was measured by a light intensity meter. The electrical power of the UV lamp was 9 W corresponding to the light intensity of 1.3 mW/cm^2. The total volume of the photoreactor is 9.5 L. Each PVL-TiO_2 thin film was placed on the inside wall of the photoreactor. The gas was circulated within a closed-system with the air pump. The relative humidity and temperature inside the photoreactor were measured continuously by using the thermo-hygrometer.

Table 1. PVL-TiO_2 formulation.

No.	Ingredients	% by weight		
		5%TiO_2	15%TiO_2	25%TiO_2
1	Concentrated latex 60% (w/w)	89.03	79.66	70.29
2	K-Oleate	0.18	0.16	0.14
3	TiO_2	5.00	15.00	25.00
4	Sulfur	2.23	1.99	1.76
5	Zinc-Diethyldithiocarbamate	1.34	1.19	1.05
6	Poly (dicyclopentadiene-co-p-cresol)	0.89	0.80	0.70
7	ZnO	1.34	1.19	1.05

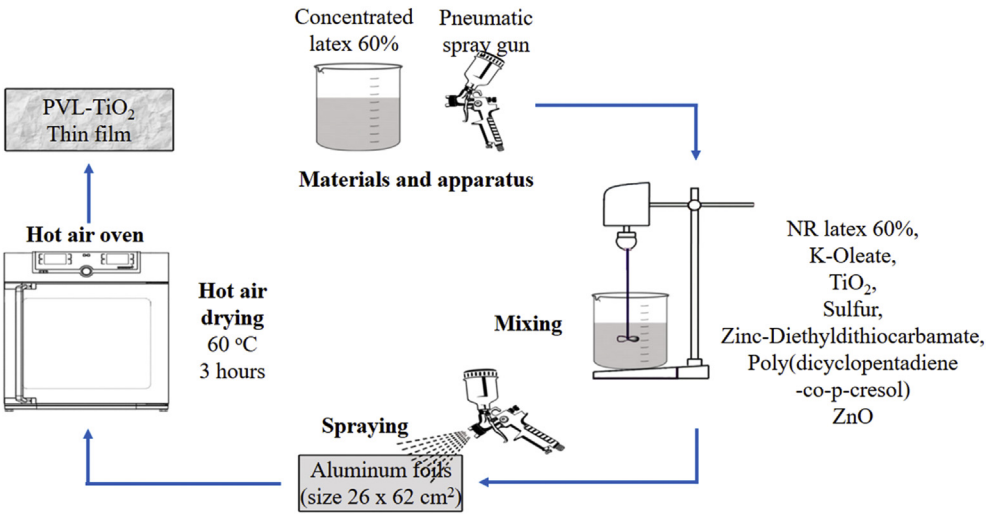

Figure 1. Preparation of PVL-TiO_2 thin films.

2.4. Benzene degradation efficiency

Liquid benzene (98%wt) at 8 μL was injected into the reactor for 2 h until the concentration of benzene inside the reactor reached 200 ppm steadily. Then the UV lamp was illuminated with the intensity of 1.3 mW/cm^2 for 5 h. Benzene-gas mixture was circulated into reactor with a rate of 3 L/min. Benzene concentrations were examined by Gas Chromatography (GC), equipped with a Flame Ionization Detector (Model 7890B, Agilent Technologies, USA). The gas sample with the volume of one milliliter was collected from the reactor using a gas tight syringe and then injected into the GC-FID with a capillary column CP sil 8. The injector temperature was set at about 150 °C and the initial column temperature was set at about 35 °C and was increased to 190 °C at a rate of 40 °C/min. Benzene degradation efficiency can be calculated using Eq. (1) [20].

$$\eta = \frac{C_0 - C}{C_0} \times 100\% \quad [1]$$

Where

η is the benzene degradation efficiency, %
C_0 is the initial concentration of substance, ppm

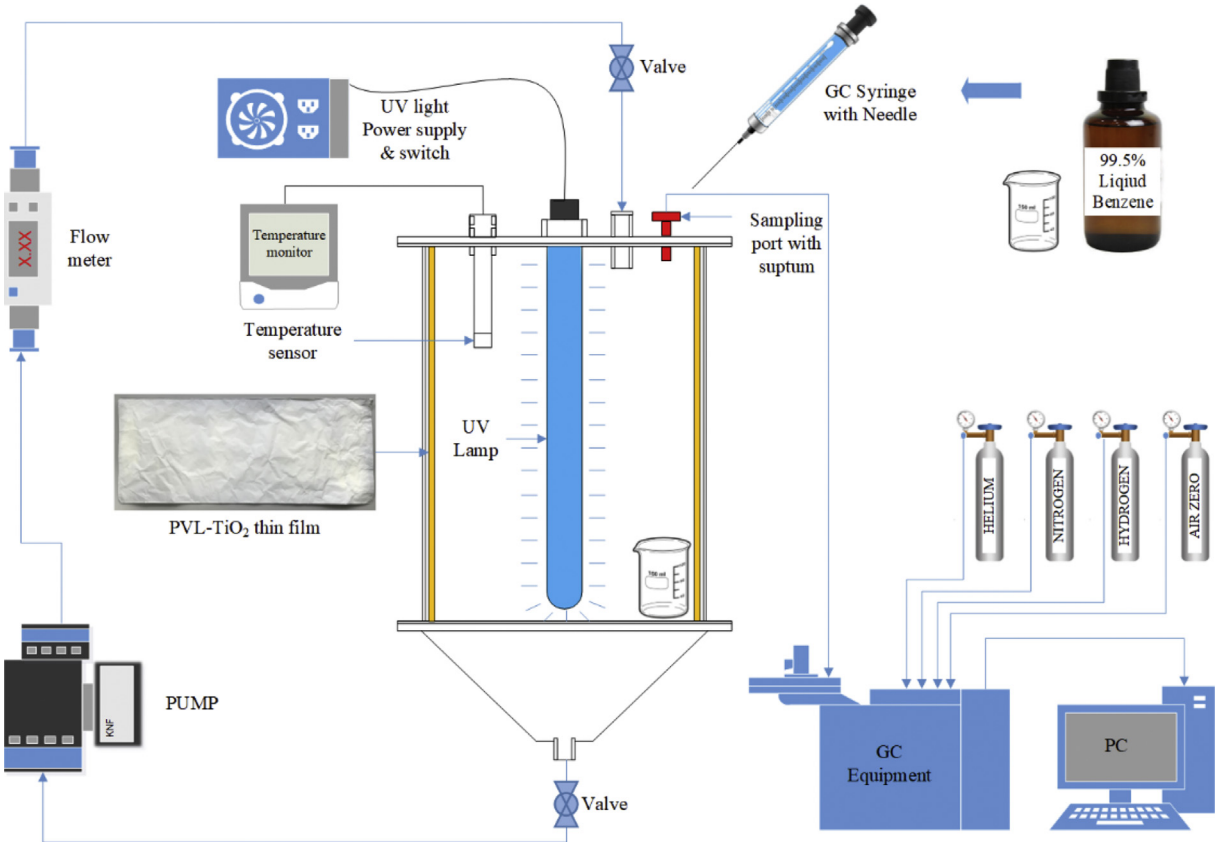

Figure 2. Schematic of photocatalytic oxidation reactor system.

C is the concentration of substance, ppm

2.5. Oxidation and carbondioxide yield rates

To determine oxidation and CO_2 yield rates, gas samples were collected at the sampling point of the reactor. The gas samples were then analyzed using GC-FID and GC-TCD for the analysis on benzene and CO_2, respectively. The analytic conditions of benzene using GC-FID as described earlier, whereas, CO_2 concentration was analysed using GC-TCD shimadzu model GC-8A TCD equipped with polar pack Q 5 M in glass column. The analytic conditions were set as follows; injection temperature 50 °C, column temperature 100 °C, TCD temperature 100 °C, current 90 mA, injection volume 0.2 mL, and gas pressure 2 kg/cm^3. The oxidation rates were calculated by Eq. (2) [21].

$$r = \frac{(C_{in} - C_{out})Q}{F \times A} \quad [2]$$

Where

C_{in} is inlet benzene concentration, ppm
C_{out} is outlet benzene concentration, ppm
Q is gas flow rate, m^3/s
A is the photocatalyst coated area, m^2
F is conversion factor (=249,376 ppm-m^3/mol, this is derived from the fact that 1 ppm = 4.01 × 10^{-6} mol/m^3)

The CO_2 yield rates were calculated using Eq. (3) [21].

$$CO_2 \ \ yield \ \ rate = \frac{C_{CO_2(\mathrm{on})} - C_{CO_2(\mathrm{off})}}{V/Q} \quad [3]$$

Where

$C_{CO_2(\mathrm{on})}$ is CO_2 concentration at outlet of photoreactor when UV lamp is on, ppm
$C_{CO_2(\mathrm{off})}$ is CO_2 concentration at outlet of photoreactor when UV lamp is off, ppm
V is volume of photoreactor, m^3
Q is gas flow rate, m^3/sec

Since VOCs are not completely mineralized to CO_2 and H_2O, and the partially oxidized VOCs remain as residual intermediates [21]. The residual intermediate was calculated as the following equation [21].

$$residual \ \ intermediate(\%) = \frac{(C_{in} - C_{out}) - [C_{CO_2(\mathrm{on})} - C_{CO_2(\mathrm{off})}]/n}{C_{in}} \quad [4]$$

Where

C_{in} is initial concentration of benzene, ppm
C_{out} is benzene concentration at the observed time, ppm
n the number of carbon atoms of benzene, 6

3. Results and discussions

As shown in Figures 3 and 4, the SEM images and the elemental mapping of the prepared PVL-TiO_2 thin films illustrate the microstructure of the dispersed TiO_2 particles in the PVL matrix. At low TiO_2 concentrations, the TiO_2 was uniformly distributed across the film surface, whereas the formation of agglomerates was observed at higher TiO_2 content (PVL-TiO_2 25)%. Since the thin films were prepared by solvent-casting of the sprayed mixed polymer solution with suspended TiO_2 onto the support surface, the shear generated to disperse the TiO_2 particles was limited to some extent. With the TiO_2 content of 5% and 15%, the thin PVL- TiO_2 film exhibited good dispersion with uniform distribution. The elemental mapping results

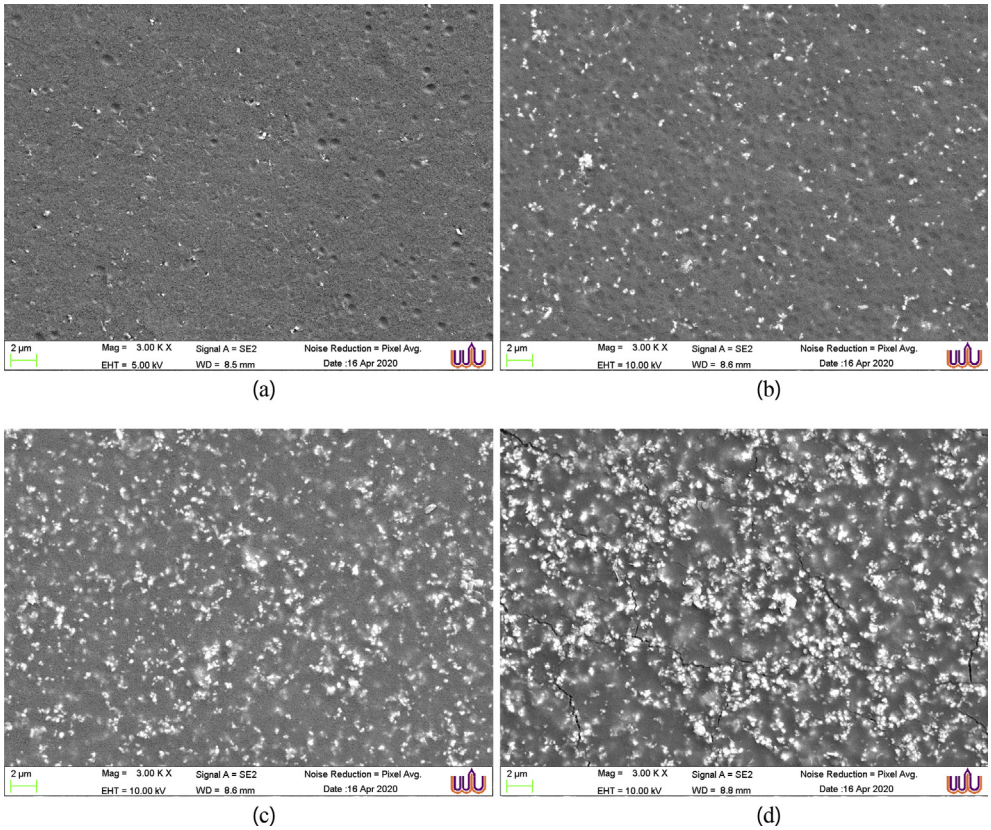

Figure 3. SEM images (10 kV, 3,000X) of (a) PVL, (b) PVL-TiO_2 5% (c) PVL-TiO_2 15% (d) PVL-TiO_2 25%.

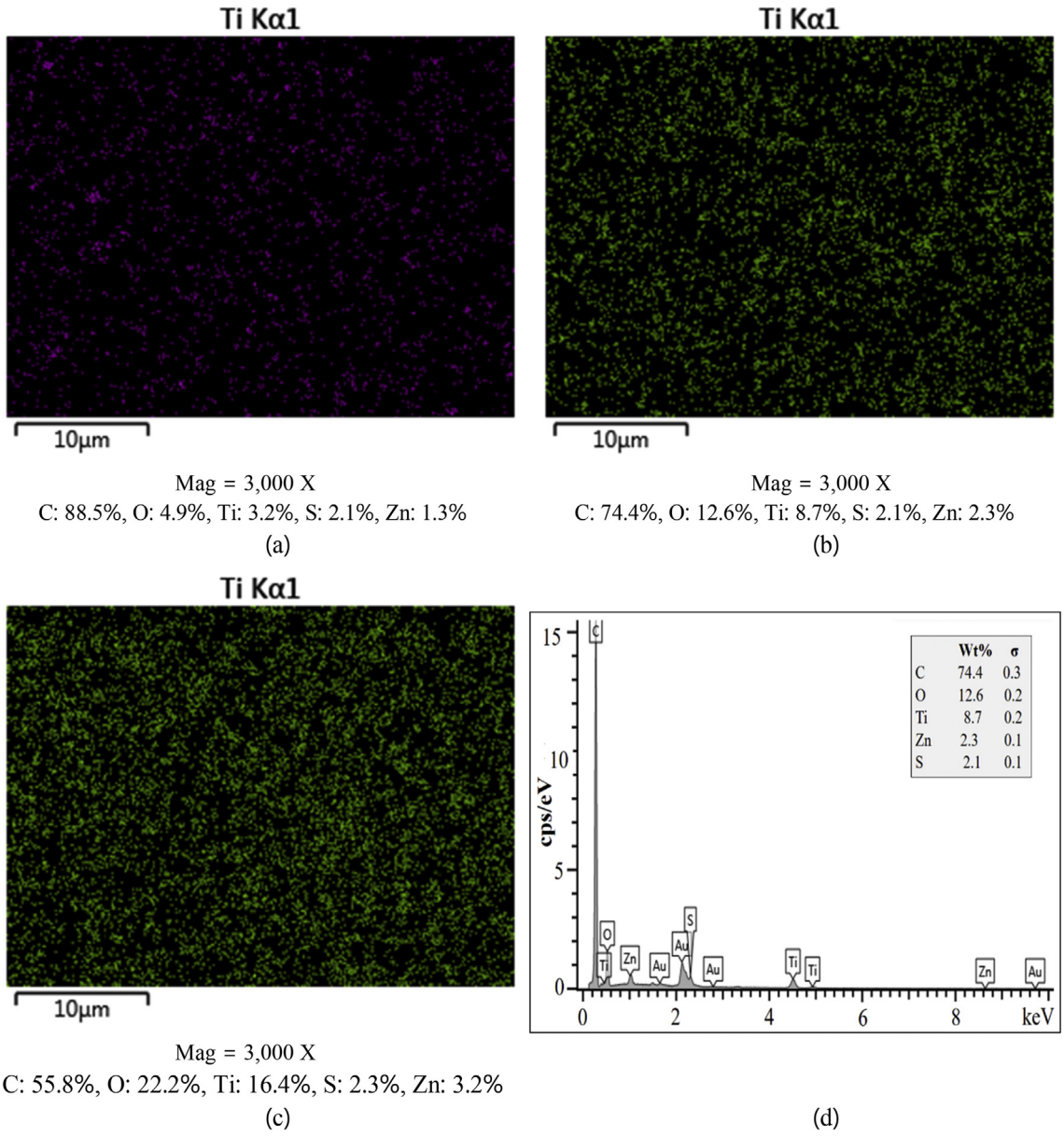

Figure 4. EDX elemental mapping results (a) PVL-TiO_2 5% (b) PVL-TiO_2 15% (c) PVL-TiO_2 25% (d) EDX results corresponding to (b).

showed that at 25% TiO_2, the primary particles tended to agglomerate and form into secondary microclusters with various sizes. A study by Pahasupanan et al. also reported a similar observation in a TiO_2-nylon 6 system [22]. EDX mapping test of the PVL and the PVL-TiO2 films are shown in the ESI R2 file. Tensile testing results using ASTM D412 at 300 % elongation can be found in the ESI R2 file.

The decomposition of PVL and PVL-TiO_2 thin films was analyzed using thermogravimetric analysis (TGA). As shown in Figure 5, the results show that weight loss occurred at around 250 °C. The decomposition of polyisoprene accounted for the lost weight at between 250 - 450 °C in PVL and PVL-TiO_2 [23]. The maximum weight loss rates in the range of 1.536–1.145 wt%/°C were attained between 380 - 382 °C TiO_2 particles enhanced the thermal stability of PVL-TiO_2 thin films due to the high decomposition temperature of its properties and also acted as a barrier for the heat transfer of PVL-TiO_2 thin films [24]. At the final testing temperature (800 °C), the relative weights remaining were approximately 3.77, 9.50, 20.86, and 28.33 % for PVL, PVL-TiO_2 5%, PVL-TiO_2 15%, and PVL-TiO_2 25%, respectively. The results from TGA analysis suggested the PVL-TiO_2 thin film could withstand the high-temperature environment in the photocatalytic reactor where the operating temperature could reach 190 °C, which was far below its decomposition temperature of around 380 °C.

The results of the specific surface area analysis (SSA) using Brunauer-Emmett-Teller (BET) are shown in Figure 6. The results showed that the increasing amount of TiO_2 increased the specific surface area of PVL-TiO_2 thin films. On the contrary, the pore diameter decreased with an increasing amount of TiO_2 content. The results were corresponding with

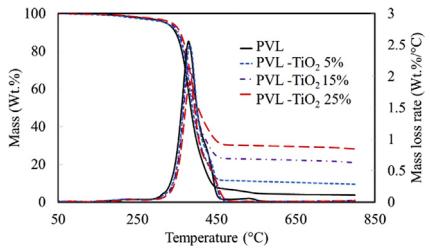

Figure 5. Thermo gravimetric analysis (TGA) and derivative thermogravimetric (DTG) of PVL and PVL- TiO_2.

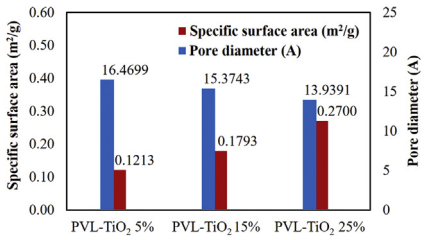

Figure 6. Specific surface area and pore diameter of PVL- TiO_2 thin films.

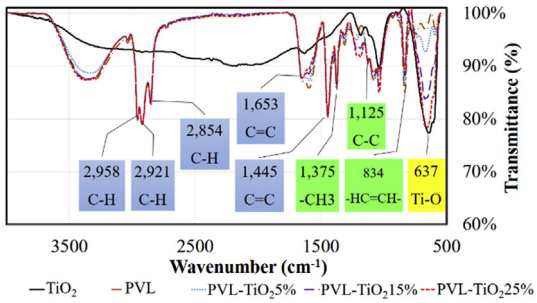

Figure 7. FTIR analysis of the PVL- TiO_2 thin film.

the morphology analysis by SEM in which at higher concentrations of TiO_2, larger size particles were formed as secondary clusters on the film surface. This resulted in higher specific surfaces areas and lower pore diameters.

The analysis of chemical functional groups of PVL, TiO_2, and PVL-TiO_2 thin film was performed using Attenuated Total Reflectance-Fourier Transform Infrared (ATR-FTIR). FTIR analysis revealed that the PVL-TiO_2 film likely possessed a chemical structure of cis-1,4. As seen in Figure 7, the peak(s) at the wavenumber of 834 cm^{-1} is associated with bending vibration of C–H in the –CH = CH– group; at 1,125 cm^{-1} for stretching vibration of C–C in the main chain; at 1,375 cm^{-1} for scissoring vibration of CH_3; at 1,445 cm^{-1} for C=C stretching; at 2,854, 2,921, and 2,958 cm^{-1} for C–H symmetrical stretching vibration; at 3,037 cm^{-1} for CH stretching vibration of –C=C– in the main chain [25, 26]. The spectrum peak at number 637 cm^{-1} represented Ti–O, in which the percentage of transmittance related to the amount of TiO_2 [27].

The results of Crystal Identification using the X-Ray Diffraction (XRD) technique are illustrated in Figure 8. The plot shows that the peaks of intensity at 2-theta (degree) occurs at 27, 41, 54, 64 and 67 (points) respectively. The height of each peak varies correlating with the amount of rutile TiO_2 content in the PVL- TiO_2 [28]. The results confirm that the TiO_2 catalyst particles well attached to the film.

Absorbance spectrums and band gap energy of PVL, PVL-TiO_2, and TiO_2 were analyzed using a UV- Visible spectrophotometer. The results of PVL and TiO_2 were compared to those absorbance spectrums of PVL-TiO_2 with 5%, 15%, and 25% TiO_2 content respectively as shows in Figure 9. Band gap energy (E_g) obtained from calculation of absorption edge wavelength (λ_{ae}) [18] are also summarized in Figure 9. It is quite clear that PVL-TiO_2 and TiO_2 has a band gap energy around 2.98–3.01 eV while PVL has a lower band gap energy at 2.88 eV. The results show that TiO_2 could

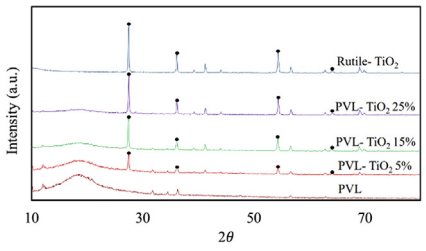

Figure 8. Crystal Identification using XRD of PVL and PVL- TiO_2.

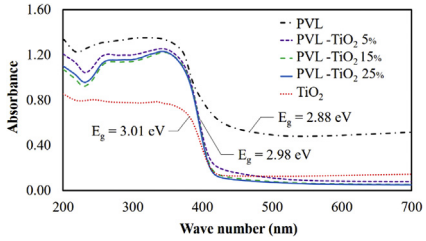

Figure 9. UV-Visible absorbance spectra and band gap energy of PVL, PVL-TiO_2 and TiO_2.

be effectively pegged at all different TiO_2 contents on PVL thin films. Results indicated that the E_g of PVL-TiO_2 5%, 15%, and 25% (2.98) were higher than that of PVL (2.88) which was induced by a higher E_g of TiO_2 (3.01). On the other hand, PVL can enhance the PCO efficiency of TiO_2 by reducing Eg, which is induced by S [29], and ZnO [30] from chemical ingredients of PVL for competency to use under visible light source.

3.1. Photo-catalytic degradation of gaseous benzene

Benzene degradation efficiency by PVL-TiO_2 thin films were carried out for 3 different contents of TiO_2 (5%, 15% and 25% TiO_2 w/w). The results are shown in Figure 10. After the UV-light was turned on, the degradation of benzene occurred due to both adsorption and photo-catalytic oxidation reaction. However, the oxidation of benzene for 15% PVL-TiO_2 thin films were higher than those of the other films (83%) while the PVL showed the maximum rate at 28%. These results can be explained that for 25% PVL-TiO_2 thin films, the larger size cluster of TiO_2 onto film surfaces may reduce the penetration of UV-light into the films, the oxidation could occur mostly on the surface, but not inside the film, resulting in lower degradation efficiencies than those of 15% PVL-TiO_2 thin films. Moreover, the larger pore diameter could enhance the mass transportation OH radicals and active molecules [31].

Theoretically, there are various intermediate species generated from the photocatalytic oxidation of benzene with TiO_2. Previous study [12] indicated that mineralization of benzene on TiO_2 catalysts proceeds via two parallel pathways. The first one is a pheolic pathway to form phenol, benzoquinone, and hydroquinone. The second one is a ring-opening pathway to producemucoaldehyde which will further decomposes rapidly. Although this study did not analyze any intermediate compounds; however, referring to photocatalytic oxidation of benzene with TiO_2, it is certain that benzene is converted to less harmful compounds which will finally result in formation of carbondioxide and water as end products [32, 33, 34, 35].

The relation of the photocatalytic oxidation rate with different dosages of PVL-TiO_2 thin films and photolysis were plotted as shown in Figure 11. The benzene degradation rate constants were obtained by fitting the experimental data using the first order reaction kinetics and rate constants. The plots indicate that the slopes of fitted straight lines using the least square method followed the first order kinetic. This is in agreement with previous research [35, 36], where the PVL and photolysis appeared to be closed to zero order. Simplified Langmuir-Hinshelwood in term of ln (C/C_0 = -kKt = -K't, at different TiO_2 dosage are shown in Table 2

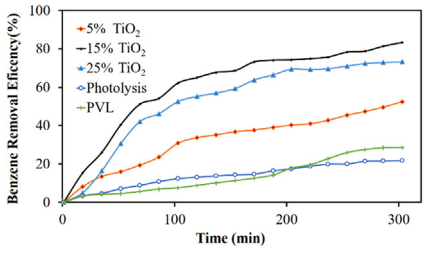

Figure 10. Benzene degradation efficiency.

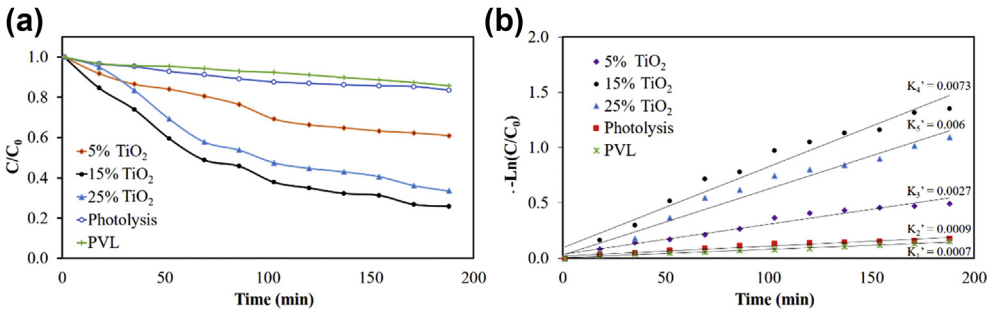

Figure 11. (a) Correlation between C/C_0 versus reaction time (b) Correlation between Ln (C/C_0) versus reaction time. (The impact of TiO_2 dosages under benzene initial concentration 200ppm, light intensity 1.3 mW/cm^2, flow rate 3 L/min).

Table 2. Simplified Langmuir-Hinshelwood in term of -ln $(C/C_0) = kKt = K't$, at different TiO_2 dosage.

Dosage	Simplified Langmuir-Hinshelwood	K′ (min^{-1})	R^2
1.Photolysis	0.0007x + 0.0088	0.0007	0.9836
2.PVL	0.0009x + 0.0212	0.0009	0.9502
3.PVL- TiO_2 5%	0.0027x + 0.0390	0.0027	0.9649
4.PVL- TiO_2 15%	0.0073x + 0.0991	0.0073	0.9665
5.PVL- TiO_2 25%	0.006x + 0.0331	0.006	0.9669

3.2. Oxidation and CO_2 yield rates

The optimum experimental conditions, based on the highest benzene degradation rate, were used to conduct additional experiment for the estimation of the oxidation, CO_2 yield rates, and the percentage of residual intermediates. PVL-TiO_2 15% thin film, 200 ppm benzene concentration, 3 L/min air flow rate, and light intensity of 1.3 mW/cm^2 were set up for the experiment. The oxidation, CO_2 yield rates, and the residual intermediates were calculated as described earlier. Figures 12 and 13 illustrate the results. As shown in Figure 12, the oxidation rate increased rapidly from the beginning to 80 min. After 80 min, the oxidation rate gradually increased. This indicated that the surface reaction occurred rapidly due to the generation of highly reactive OH radicals. The OH radicals were generated after water molecules or OH^- adsorbed on the photocatalytic film surface and reacted with photogenerated holes in the valence band [32].

From Figure 12, the CO_2 yield rates increased as the increasing of the oxidation rate and time. The controlling rate of CO_2 yield is probably the surface reaction. It was seen that the CO_2 yield rate was relevant to the apparent oxidation rate of benzene or a secondary intermediate. Theoretically, benzene can completely be converted to CO_2 and H_2O, however, residual intermediates can be found for incomplete mineralization. Figure 13 shows the percentage of residual intermediates versus time. As seen in the Figure, the amount of residual intermediate increased rapidly from the beginning up to 80 min. Hereafter, the intermediates increased slowly which corresponded to the oxidation rates. For PCO, accumulation of residual intermediates can occur on the active site and the gas phase, resulting in increasing of residual intermediates [32]. In order to reduce the amount of residual intermediates, the longer reaction time is required for the complete mineralization and oxidation [21].

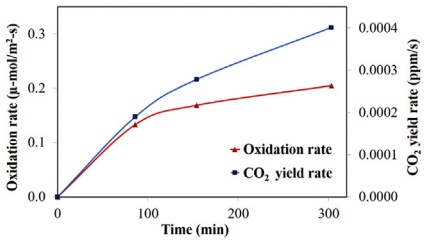

Figure 12. The oxidation and the CO_2 yield rates versus time.

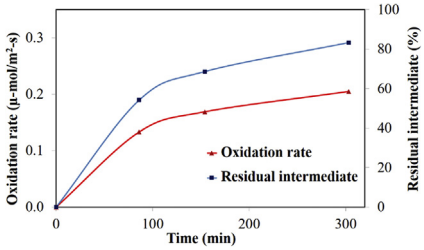

Figure 13. The percentage of residual intermediates versus time.

4. Conclusions

Pre-vulcanized latex impregnated with TiO_2 (PVL-TiO_2) thin film was successfully synthesized by immobilizing titanium dioxide (TiO_2) on natural rubber with chemical reagents in order to transform natural rubber to pre-vulcanized latex for better properties and practically be used as indoor air treatment application. SEM illustrated that TiO_2 particles were uniformly distributed all over the surface of thin film as the confirmed results from FTIR. The type of TiO_2 crystalline structure was rutile that confirmed by XRD results. Compared to PVL, PVL- TiO_2 thin films; tensile strength obviously improved because of TiO_2, which can reinforce the strength of natural rubber substrate. The thermal stability of PVL-TiO_2 thin film suggested that the film can be used under rather high temperature conditions. By the results of UV-Visible absorbance spectra, PVL-TiO_2 thin films, which consisted of sulfur and zinc, had lower energy band gap than that of TiO_2. Finally, the photo-catalytic degradation efficiencies of gaseous benzene were achieved up to 80% after 5 h of UV light illumination. The dosage of TiO_2 increased the treatment capacity of the photo-catalytic degradation rate until it reached the concentration of 15% PVL-TiO_2 thin films. At this optimal TiO_2 content (15%), the active TiO_2 particles were well dispersed in the polymer matrix with good uniformity, yielding high specific surface area essential for adsorption process of the moisture and benzene involving in the photo-oxidation reactions. It is certainly found that benzene is converted by the adsorption and photocatalytic mechanisms onto the PVL-TiO_2 thin films to less harmful compounds which can further oxidized to finally form water and carbondioxide as end products.

Declarations

Author contribution statement

Wipawee Dechapanya: Conceived and designed the experiments; Analyzed and interpreted the data; Contributed reagents, materials, analysis tools or data; Wrote the paper.

Peerapol Kaoien: Performed the experiments; Analyzed and interpreted the data; Wrote the paper.

Attaso Khamwichit: Analyzed and interpreted the data; Wrote the paper.

Kowit Suwannahong: Contributed reagents, materials, analysis tools or data; Wrote the paper.

Funding statement

This work was financially supported by Research Grant No. WU60104 and partially supported by the New Strategic Research (P2P) project (phase 2), Walailak University, Thailand.

Competing interest statement

The authors declare no conflict of interest.

Additional information

Supplementary content related to this article has been published online at https://doi.org/10.1016/j.heliyon.2020.e03912.

References

[1] E.R. Rene, S. Kar, J. Krishnan, K. Pakshirajan, M.E. López, D.V.S. Murthy, T. Swaminathan, Start-up, performance and optimization of a compost biofilter treating gas-phase mixture of benzene and toluene, Bioresour. Technol. 190 (2015) 529–535.

[2] K. Jagannathan, T. Swaminathan, Removal of gas-phase benzene in immobilized photocatalytic reactor, Macedonian J. Chem. Chemical Eng. 30 (2) (2011) 221–228.

[3] M. Wongaree, S. Chiarakorn, S. Chuangchote, T. Sagawa, Photocatalytic performance of electrospun CNT/TiO2 nanofibers in a simulated air purifier under visible light irradiation, Environ. Sci. Pollut. Control Ser. 23 (21) (2016) 21395–21406.

[4] M. Farhadian, D. Duchez, C. Vachelard, C. Larroche, BTX removal from polluted water through bioleaching processes, Appl. Biochem. Biotechnol. 151 (2–3) (2008) 295–306.

[5] B. Belaissaoui, Y. Le Moullec, E. Favre, Energy efficiency of a hybrid membrane/condensation process for VOC (Volatile Organic Compounds) recovery from air: a generic approach, Energy 95 (2016) 291–302.

[6] W. Wang, X. Ma, S. Grimes, H. Cai, M. Zhang, Study on the absorbability, regeneration characteristics and thermal stability of ionic liquids for VOCs removal, Chem. Eng. J. 328 (2017) 353–359.

[7] Z. Luo, L. Li, C. Wei, H. Li, D. Chen, Role of active oxidative species on TiO_2 photocatalysis of tetracycline and optimization of photocatalytic degradation conditions, J. Environ. Biol. 36 (4) (2015) 837–843.

[8] K. Suwannahong, W. Sanongraj, J. Kruenate, S. Phibanchon, S. Jawjit, W. Khamwichit, Photo catalytic oxidation degradation of volatile organic compound with nano-TiO2/LDPE composite film, Int. Scholarly Scientific Res. Innovation 7 (1) (2014) 65–69.

[9] R. Ahmad, Z. Ahmad, A.U. Khan, N.R. Mastoi, M. Aslam, J. Kim, Photocatalytic systems as an advanced environmental remediation: recent developments, limitations and new avenues for applications, J. Environ. Chem. Eng. 4 (4) (2016) 4143–4164.

[10] J. Lu, L. Lan, X.T. Liu, N. Wang, Xiaolei Fan, Plasmonic Au nanoparticles supported on both sides of TiO_2 hollow spheres for maximising photocatalytic activity under visible light, Front. Chem. Sci. Eng. 13 (4) (2019) 665–671.

[11] V. Etacheri, C. Di Valentin, J. Schneider, D. Bahnemann, S.C. Pillai, Visible-light activation of TiO2 photocatalysts: advances in theory and experiments, J. Photochem. Photobiol. C Photochem. Rev. 25 (2015) 1–29.

[12] T.D. Bui, A. Kimura, S. Higashida, S. Ikeda, M. Matsumura, Two routes for mineralizaing benzene by TiO_2-photocatalyzed reaction, Appl. Catal. B Environ. 107 (2011) 119–127.

[13] C. Tharasawatpipat, K. Suwannahong, J. Kruenate, T. Kreetachat, Removal of VOCs by photocatalytic oxidation using nano-TiO2/PLA biocomposite, J. Environ. Biol. 36 (3) (2015) 617–621.

[14] C. Sriwong, S. Wongnawa, O. Patarapaiboolchai, Photocatalytic activity of rubber sheet impregnated with TiO2 particles and its recyclability, Catal. Commun. 9 (2) (2008) 213–218.

[15] C. Sriwong, S. Wongnawa, O. Patarapaiboolchai, Rubber sheet strewn with TiO2 particles: photocatalytic activity and recyclability, J. Environ. Sci. 24 (3) (2012) 464–472.

[16] C. Sriwong, S. Wongnawa, O. Patarapaiboolchai, Recyclable thin TiO 2-embedded rubber sheet and dye degradation, Chem. Eng. J. 191 (2012) 210–217.

[17] A. Ali Shah, F. Hasan, Z. Shah, N. Kanwal, S. Zeb, Biodegradation of natural and synthetic rubbers: a review, Int. Biodeterior. Biodegrad. 83 (2013) 145–157.

[18] J.C.S. Costa, R.J.S. Taveira, C.F.R.A.C. Lima, A. Mendes, L.M.N.B.F. Santos, Optical band gaps of organic semiconductor materials, Opt. Mater. 58 (2016) 51–60.

[19] Crane, Flow of Fluids Throuh Valves, Fittings and Pipe. Technical Paper No.410M, New York, Crane CO, 1998, p. 128.

[20] T.D. Pham, B.K. Lee, C.H. Lee, The advanced removal of benzene from aerosols by photocatalytic oxidation and adsorption of Cu-TiO2/PU under visible light irradiation, Appl. Catal. B Environ. 182 (2016) 172–183.

[21] Yu Kuo-Pin, G.W.M. Lee, Wei-Ming Huang, C. Wu, S. Yang, The correlation between photocatalytic oxidation performance and chemical/physical properties of indoor volatile organic compounds, Atmos. Environ. 40 (2006) 375–385.

[22] T. Pahasup-anan, K. Suwannahong, W. Dechapanya, R. Rangkupan, Fabrication and photocatalytic activity of TiO_2 composite membranes via simultaneous electrospinning and electrospraying process, J. Environ. Sci. (China) (2017) 1–12.

[23] T. Pojanavaraphan, R. Magaraphan, Prevulcanized natural rubber latex/clay aerogel nanocomposites, Eur. Polym. J. 44 (7) (2008) 1968–1977.

[24] P. Toh-ae, B. Junhasavasdikul, N. Lopattananon, Mechanical properties and stability towards heat and UV irradiation of natural rubber/nanotitanium dioxide composites, Procedia Chemistry 19 (2016) 139–147.

[25] D. Chen, H. Shao, W. Yao, B. Huang, Fourier transform infrared spectral analysis of polyisoprene of a different microstructure, Int. J. Polym. Sci. 2013 (2013) 1–5.

[26] B.H.M. Fan, D. Dai, Fourier transform infrared spectroscopy for natural fibres, Fourier Transform-Material. Analysis (2012).

[27] M.B. Askari, Z. Tavakoli Banizi, M. Seifi, S. Bagheri Dehaghi, P. Veisi, Synthesis of TiO2 nanoparticles and decorated multi-wall carbon nanotube (MWCNT) with anatase TiO2 nanoparticles and study of optical properties and structural characterization of TiO2/MWCNT nanocomposite, Optik 149 (2017) 447–454.

[28] A. He, G. Chen, J. Chen, J. Peng, C. Srinivasakannan, R. Ruan, A novel method of synthesis and investigation on transformation of synthetic rutile powders from Panzhihua sulphate titanium slag using microwave heating, Powder Technol. 323 (2018) 115–119.

[29] Z. Chen, J. Ma, K. Yang, S. Feng, W. Tan, Y. Tao, M. Huihui, K. Yong, Preparation of S-doped TiO2-three dimensional graphene aerogels as a highly efficient photocatalyst, Synth. Met. 231 (2017) 51–57.

[30] D. Sethi, R. Sakthivel, ZnO/TiO2 composites for photocatalytic inactivation of Escherichia coli, J. Photochem. Photobiol. B Biol. 168 (2017) 117–123.

[31] H.A. Mahmoud, K. Narasimharao, T.T. Ali1, K.M.S. Khalil, Acidic peptizing agent effect on anatase-rutile ratio and photocatalytic performance of TiO_2 nanoparticles, Nanoscale Res. Lett. 13 (2018) 48.

[32] F.A. Hernandez-Carcia, G. Torres-Delgado, R. Castanedo-Perez, O. Zelaya-Angel, Gaseous benzene degradation by photocatalysis using $ZnO+Zn_2TiO_4$ thin films obtained by sol-gel process, Environ. Sci. Pollut. Res. 23 (2016) 13191–13199.

[33] D. Cherni, N. Moussa, M.F. Nsib, A. Olivo, M. Signoretto, L. Prati, A. Villa, Photocatalytic degradation of ethybenzene in gas phase over N and NF doped TiO_2 catalysts, J. Mater. Sci. Mater. Electron. 30 (2019) 18919–18926.

[34] A.J. Jafari, R.R. Kalantari, M. Kermani, M.H. Firooz, Photocatalytic oxidation of benzene by ZnO coated on glass plates under simulated sunlight, Chem. Pap. 73 (2019) 635–644.

[35] A. Derakhshan-Nejad, H.A. Rangkooy, M. Cheraghi, R.J. Yengejeh, Removal of ethyl benzene vapor pollutant from the air using TiO_2 nanoparticles immobilized on the ZSM-5 zeolite under UVradiation, J. Environ. Health Sci. Eng. (2020).

[36] M. Malayeri, F. Haghighat, C.S. Lee, Modeling of volatile organic compounds degradation by photocatalytic oxidation reactor in indoor air: a review, Build. Environ. 154 (2019) 309–323.